NOVEL INTEGRATED ACTIVE AND PASSIVE CONTROL OF FLUID-BORNE NOISE IN HYDRAULIC SYSTEMS

Min Pan* **Chenggang Yuan** **Beichen Ding** **Andrew Plummer**

Centre for Power Transmission and Motion Control
Department of Mechanical Engineering
University of Bath
Bath, United Kingdom, BA2 7AY

*Email: m.pan@bath.ac.uk

ABSTRACT

Fluid-borne noise (FBN) is a major contributor to structure-borne noise (SBN) and air-borne noise (ABN) in hydraulic fluid power systems and could lead to increased fatigue in system components. FBN is caused by the unsteady flow generated by pumps and motors and propagates through the system resulting in SBN and ABN. New hydraulic technologies such as digital switched hydraulic converters are also barriered by the unavoidable FBN. This article reports on a novel integrated FBN attenuation approach, which employs a hybrid control system by integrating an active feedforward noise attenuator with passive tuned flexible hoses. The active system which consists of adaptive notch filters using a variable step-size filtered-X Least Mean Squares algorithm is used to control a newly designed high-force high-bandwidth piezoelectric actuator in order to attenuate the dominant narrowband pressure ripples. The passive hose is tuned in the frequency domain and used to cancel the high-frequency pressure ripples. A time-domain hose model considering coupling of longitudinal wall and fluid waves was used to model the flexible hose in the integrated control system. Very good FBN cancellation was achieved by using the proposed integrated control approach both in simulation and experiments. It can be concluded that the active attenuator with passive flexible hoses can form an effective, cost-efficient and practical solution for FBN attenuation. The problem of high noise levels generated by hydraulically powered machines has risen significantly in awareness within industry and amongst the general public, and this work constitutes an important contribution to the sustainable development of low noise hydraulic fluid power machines.

NOMENCLATURE

A_d	amplitude of the fluid-borne noise
B_E	effective bulk modulus of fluid in the hose
$d(n)$	the primary noise
$e(n)$	residual error signal
E_x	axial stiffness of the hose
f_0	fundamental frequency of the fluid-borne noise
F_i	Fourier transformed forward travelling waves
F_a	force of the piezo actuator
f_i	forward travelling waves
f_i'	delayed and attenuated forward travelling waves
G_i	Fourier transformed backward travelling waves
g_i	backward travelling waves
g_i'	delayed and attenuated backward travelling waves
k_v	force/voltage coefficient
k_x	actuator stiffness
L	the length of the tube
N_i	modal ratio between the wall and fluid velocity of wave i
P	Fourier transformed pressure
$P(z)$	the plant between the noise source and the error sensor
r_b	internal radius of the hose
r_r	mean reinforcement radius
$S(s)$	continuous secondary path transfer function
$S(z)$	discrete time secondary path transfer function (secondary path dynamics)
U	Fourier transformed fluid velocity averaged across the passageway section
V	applied voltage for the piezo actuator
V_a	amplifier input voltage
W	Fourier transformed wall velocity
$\mathbf{w}(n)$	weight vector
$W(z)$	the adaptive filter
w_0, w_1	weights of adaptive notch filter
$W_i(t)$	the weighting function for wave i
x	the distance along the hose
$x(n)$	reference signal
$\mathbf{x}(n)$	reference signal vector
x_p	extension of the piezo actuator
$y(n)$	output of the adaptive filter
Z_i	characteristic impedance (ratio of pressure wave to fluid velocity wave)
α	leakage factor
γ_i	propagation constant for wave i
ζ	damping ratio of secondary path

η	small user-defined step size
ξ	positive constant close to 1
ρ	fluid density
ϕ_d	phase of the fluid-borne noise
ω	natural frequency of the secondary path
ω	angular frequency
$\hat{S}(z)$	estimated secondary path dynamics
$y'(n)$	filtered output of the adaptive filter
γ_i	propagation constant for wave *i*
$\overline{\gamma}_i$	defined as γ_i / ω
ν_x	axial Poisson's ratio
τ	time for convolution integral
$x_0'(n)$, $x_0'(n)$	filtered reference signals for the two-weight adaptive notch filter
$x_{m,0}'(n)$, $x_{m,1}'(n)$	filtered reference signals for parallel two-weight adaptive notch filter *M*
Δt	sampling time step
μ	constant convergence rate
$\mu(n)$	variable filter step size
$\boldsymbol{\mu}(n)$	step size vector

1. INTRODUCTION

Fluid-borne noise (FBN) is a major contributor to air-borne noise (ABN) and structure-borne noise (SBN) in hydraulic power systems as well as leading to increased fatigue in pumps, motors, valves and actuators. Noise can generally be divided into broadband and narrowband noise according to the energy distribution. The cyclic mechanism of pumps and motors generates periodic noise in the system (i.e. narrowband), and instability and cavitation in valves introduce broadband noise [2]. New energy-efficient hydraulic devices, such as electrohydrostatic actuators and switched inertance hydraulic converters (SIHC) exhibit particularly significant noise problems due to the nature of their control and design [3-9]. Passive FBN attenuators, such as Inline Pulse-Tone™ Shock Suppressors developed by Parker Hannifin [10], silencers, pulsation dampers and accumulators are widely used by industries. These devices are effective to high-frequency noise but normally add extra compliance to the system that can impair the system dynamic response.

Active noise cancellation technique provides a new approach to attenuate FBN. Previous research shows the active attenuator can be effective at a wide range of cancellation frequencies without significantly affecting hydraulic system dynamics [11]. However, this new technology is still in its infancy due to the limitations of the active component regarding the bandwidth, available force and response time.

Over 30 years ago, Rebel used a fast-response servo-valve and an auxiliary pump to generate high-frequency flow fluctuations to attenuate FBN [12]. This work is believed to be the first attempt of using the active noise control approach which employed a secondary source for hydraulic pressure pulsation attenuation. A radial three-piston pump rotating at a speed of 2000 rpm was used to validate Rebel's active attenuator. The results showed that 9 dB reduction was successfully achieved using the designed open-loop controller; while 17 dB noise reduction was achieved using a closed-loop controller. However, the bandwidth of the cancellation was limited to 50 Hz as the use of the servo valve. The overall system efficiency is low, which is caused by the pressure drop through the servo valve. Moreover, the cost of a high-bandwidth servo-valve could be higher than a piston pump. The authors believe that a fast response, adaptive controlled and energy-efficient active attenuator could provide a better solution. In 1999, an active fluid wave attenuator was successfully designed to generate a controlled flow wave with a same amplitude but in anti-phase to the original pressure ripple (primary noise). A circumferential ring of Lead Zirconate Titanate (PZT) stacks was arranged in series with the primary noise as the active component connecting along the pipe to generate an axisymmetric plane wave in the fluid through radial motion coupling [13]. This was the first use of piezoelectric actuation for flow ripple attenuation. Later, at the University of Bath, a servo-valve was used again by Wang et al with an adaptive control algorithm for FBN cancellation. Similar to Rebel's conclusions, the effective cancellation bandwidth is low due to the bandwidth of the servo valve. However, the team has proven the principle of adaptive control methodology for active FBN cancellation [14]. The team also found that the active controller can be unstable due to the contamination sensitivity of the servo valve. Recently the active adaptive control approach has been applied to FBN cancellation in hydraulic pipelines and a switched inertance hydraulic converter using a piezoelectric valve by Pan *et al*. The results showed very good FBN cancellation and the active controller is robust subject to the varying loading conditions [11,15-16]. Xu *et al* investigated the flow ripple reduction of axial piston pump using a variety of methods including the combination of cross angle and pressure relief grooves [17], valve plate optimization [18] and nonuniform distribution of pistons [19]. Good FBN cancellation has been achieved. It is noticed that the flow ripple amplitude can be reduced by more than 50% in average by using nonuniform distribution of pistons.

This article is an extended version of a paper presented at the BATH/ASME 2018 Symposium on Fluid Power and Motion Control [1]. This article investigates on the performance of a new integrated FBN controller that combines an active feedforward noise attenuator and passive tuned flexible hoses together to provide an effective solution for FBN attenuation. Hydraulic flexible hoses are essential to most fluid power systems, and they can effectively damp the pressure pulsations if they are suitably tuned as passive noise attenuators. Tuned hoses can benefit the system FBN reduction without any extra cost. However, the hose length and diameter are normally selected based on other constraints in most industrial cases. The new integrated active and passive control approach is proposed and presented in Section 2. The integrated approach includes a tuning method for passive flexible hoses in Section 2.1 and an active noise attenuator that is designed to cancel the dominant harmonic pressure pulsations in the fluid line in Section 2.2. The passive

flexible hose is tuned to attenuate the residual high-frequency pulsations. Theoretical simulation and experimental validation were presented in Section 3 and 4. An external gear pump is used as the primary noise of the system. The Speedgoat real-time simulation and testing control platform was used to implement the proposed active controller. Discussion and conclusions were presented in Section 5 and 6.

2. INTEGRATED CONTROL OF FLUID BORNE NOISE

The schematic of an integrated active and passive fluid-borne noise (FBN) control system is shown in figure 1, where a flexible hose is arranged at the outlet of the primary noise source (pump or digital hydraulic system) to attenuate the high frequency noise. An active actuator is designed to attenuate the dominant pressure pulsations, whilst the passive flexible hose is tuned to cancel the high-frequency ripples. The principles of active noise control systems [16] are employed to develop the active controller on an active actuator. A tachometer is installed upstream and used to measure the speed of the pump which is then used to calculate the frequency of the narrowband FBN. The estimated frequency is fed into a signal generator to generate reference signals having the same frequency as the measured FBN (primary noise). An adaptive algorithm is developed and applied in the active controller located in the downstream pipeline in order to attenuate the dominant harmonic pulsations (narrowband FBN). The physical dynamics between the measured transducer and the input of the active controller is called the secondary path. With this new system design based on the integration of an active attenuator and passive hose tuning, the fluid-borne noise can potentially be significantly reduced for a wide range of high frequencies while the system continues to maintain a very good dynamic response.

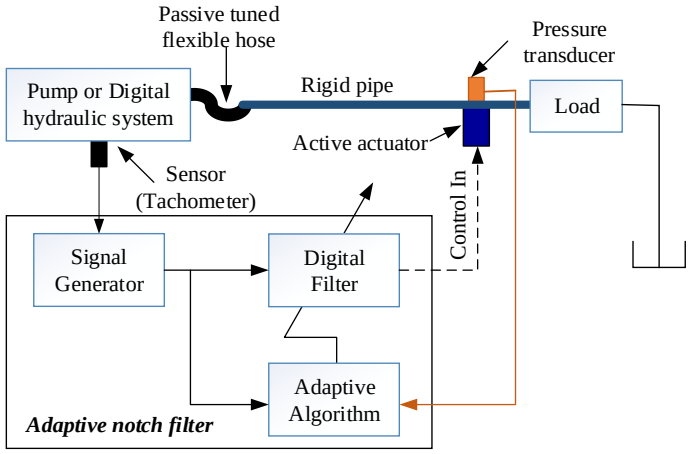

FIGURE 1. The schematic of an integrated fluid-borne noise control system

2.1 Passive tuned flexible hoses

Flexible hose dynamics have a significant effect on noise and vibration characteristics of hydraulic systems. In most of cases, hoses have been modelled in the time domain as simple rigid tubes with a reduced oil bulk modulus. This is only accurate for a very limited bandwidth and does not capture the true behaviour of longitudinal waves in the wall and in the liquid [20].

The dynamic behavior of liquid in a flexible hose is difficult to model because of complex interactions between the liquid and the hose wall [18]. Due to the increased flexibility of the hose wall, longitudinal waves in the wall and in the liquid are closely coupled. They behave at two different wave speeds. In addition, a high level of damping is expected due to the viscoelastic materials in the hose wall. Research has been carried out into the modelling of flexible hoses in the frequency and time domains at the University of Bath [21-25]. To investigate detailed wave behaviour in a hose, Taylor developed a time-domain hose model based on a one-dimensional finite element method (FEM) [24]. The model is effective but requires detailed static and dynamic material properties for a range of pressures. Johnston developed a flexible hose model in the time domain based on the transmission line method (TLM), which includes coupling of longitudinal wall and fluid waves and the corrections for viscoelastic relaxation and non-linearities [21]. The fluid velocity, pressure, and axial wall velocity in the frequency domain can be expressed as:

$$U = F_1 e^{-\gamma_1 x} + G_1 e^{-\gamma_1 (L-x)} + F_2 e^{-\gamma_2 x} + G_2 e^{-\gamma_2 (L-x)} \quad (1)$$

$$P = Z_1 (F_1 e^{-\gamma_1 x} - G_1 e^{-\gamma_1 (L-x)}) + Z_2 (F_2 e^{-\gamma_2 x} - G_2 e^{-\gamma_2 (L-x)}) \quad (2)$$

$$W = N_1 (F_1 e^{-\gamma_1 x} + G_1 e^{-\gamma_1 (L-x)}) + N_2 (F_2 e^{-\gamma_2 x} + G_2 e^{-\gamma_2 (L-x)}) \quad (3)$$

where F_1 and F_2 are the two waves travelling in the forward direction, G_1 and G_2 represent the waves travelling in the reverse direction, N_1 and N_2 are modal ratio between the wall and fluid velocity for forward wave and backward wave, x is the distance along the hose, L is the length of the tube and γ_1 and γ_2 are the wave propagation constants.

The propagation constants are the solutions $\pm\bar{\gamma}_1, \pm\bar{\gamma}_2$ of

$$A_0 \bar{\gamma}^4 + A_1 \bar{\gamma}^2 + A_2 = 0 \quad (4)$$

where [18]

$$A_0 = \frac{E_x r_b^2}{\rho r_r^2} \quad (5)$$

$$A_1 = \pi r_r^2 \left(1 - 2\nu_x - \frac{r_b^2}{r_r^2}\right)^2 + \frac{E_x}{B_E} + \frac{m}{\rho}\frac{r_b^2}{r_r^2} \quad (6)$$

$$A_2 = \frac{m}{B_E} \quad (7)$$

where E_x is the axial stiffness of the hose, r_b is the internal radius of the hose, r_r is the mean reinforcement radius, ρ is the fluid density, ν_x is the axial Poisson's ratio and B_E is the effective bulk modulus of fluid in the hose, m is the weighting function number which could be modified to incorporate non-linearity [21].

Z_i is the characteristic impedance, the ratio of pressure wave to fluid velocity wave, of wave i,

$$Z_i = \frac{\rho}{j\bar{\gamma}_i} \tag{8}$$

N_i is the modal ratio between the wall and fluid velocity for wave i,

$$N_i = \frac{(r_b^2 / r_r^2)\bar{\gamma}_i^2 B_E + \rho}{(1 - r_b^2 / r_r^2 - 2\nu_x)\bar{\gamma}_i^2 B_E} \tag{9}$$

From equation (1) the fluid velocity at $x = 0$ is

$$U_A = F_1 + G_1 e^{-\gamma_1 L} + F_2 + G_2 e^{-\gamma_2 L} \tag{10}$$

At $x = L$,

$$U_B = F_1 e^{-\gamma_1 L} + G_1 + F_2 e^{-\gamma_2 L} + G_2 \tag{11}$$

Equation (10) and (11) can be transformed to the time domain as:

$$u_A(t) = f_1(t) + g_1'(t) + f_2(t) + g_2'(t) \tag{12}$$

$$u_B(t) = f_1'(t) + g_1(t) + f_2'(t) + g_2(t) \tag{13}$$

where $g_i'(t)$ and $f_i'(t)$ represent the delayed and attenuated waves, and can be obtained using a convolution integral:

$$g_i'(t) = \int_{-\infty}^{\infty} g_i(t+\tau) W_i(-\tau) d\tau \tag{14}$$

$$f_i'(t) = \int_{-\infty}^{\infty} f_i(t+\tau) W_i(-\tau) d\tau \tag{15}$$

where $W_i(t)$ is the weighting function for wave i.

$$W_i(\tau) = F^{-1}(e^{-\gamma_i L}) \tag{16}$$

$W_i(t)$ can be approximated in the time domain using the summation method and the recursive method. Compromise should be made between the accuracy and computation complexity of the model when approximating the weighting function. A detailed derivation of the approximation can be found in Ref. [21]. The recursive method is used in this work for modelling the hose in the time domain. The model is able to predict very rapid transients accurately, but it also requires knowledge of the material properties, which are sensitive to the temperature, pressure and curvature. Johnston *et al* also investigate the static and dynamic properties of a range of hoses, providing the necessary parameter values for modelling [26].

The hose characteristics are also investigated in the frequency domain using software '*Prasp*' [27]. The results are used for tuning hose parameters, which are used in the time-domain hose model stated above. Commercial double layer steel braid hoses with different lengths and diameters supplied by Parker Hannifin are used as passive FBN attenuating components. Different tube length and diameter will affect the system resonant frequency and dynamic response. Figure 2 shows the amplitude ratio (quotient) of the pressure at the outlet of a rigid pipe and the outlet of the pump with different hose lengths. The rigid pipe length is 1 m and the diameter is 10 mm. The strongest resonant frequency is 320 Hz without a hose. The resonant frequency decreases with the increase of the hose length. For example, the resonant frequency reduced to 100 Hz with a length of 1.7 m hose. As can be seen, using the passive flexible hoses with lengths of 1.1 m and 1.7 m, the high-frequency ripples can be effectively attenuated. The tuned hoses (1.1m and 1.7m with an internal diameter of 12.5 mm) are used with the active FBN attenuator to form a new integrated FBN control system. Table 1 shows the hose properties.

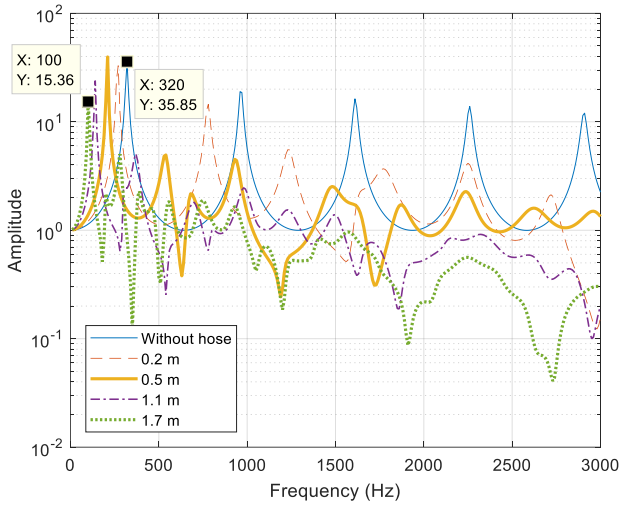

FIGURE 2. Amplitude ratio of the pressure at the outlet of the rigid pipe and the outlet of the pump with and without hoses

TABLE 1. Hose properties

Internal diameter $2r_b$ (mm)	Reinforcement diameter $2r_r$ (mm)	Rated pressure (bar)	Mass per unit length m (kg/m)	Length l (m)
12.5	19.0	275	0.68	1.1
12.5	19.0	275	0.68	1.7

In the tuning procedure, it is crucial to maintain a low overall amplitude ratio at high frequencies when a flexible hose is used. This can ensure good attenuation at a wide range of high frequencies, reduce the power requirements of the active attenuator and avoid high noise levels when the active attenuator is inactive. In addition, it can improve controller stability because the system dynamics are more highly damped at those frequencies.

2.2 Active fluid-borne noise controller

An active noise control (ANC) system employing the classic filtered-X Least Mean Square (FXLMS) algorithm is shown in Figure 3. The FXLMS algorithm is developed from the conventional LMS filter which was originally proposed by Widrow and Hoff [28]. The detailed derivation and analysis of the LMS algorithm can be found in Ref. [29].

The primary path $P(z)$ is the plant between the noise source and the error sensor, which is the pressure transducer in Figure 1. The adaptive filter $W(z)$ updates its coefficients to track the variations of the primary path $P(z)$. When the length of $W(z)$ equals two, the FXLMS adaptive notch filter is formed, which can be used for narrowband noise cancellation. In hydraulic

systems, the primary noise $d(n)$ is the FBN generated from the pump or by the switching of digital hydraulic valves with a fundamental frequency f_0:

$$d(n) = A_d \sin(2\pi f_0 n\Delta t + \phi_d) \tag{17}$$

where A_d is the amplitude, and ϕ_d is the phase.

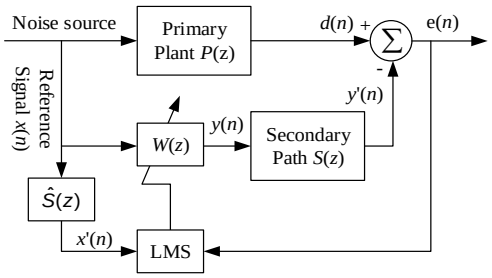

FIGURE 3. Block diagram of an active noise control system using FXLMS adaptive algorithm

The two adaptive weights are iterated by the following equations:

$$w_0(n+1) = \alpha w_0(n) + \mu x_0'(n) e(n) \tag{18}$$

$$w_1(n+1) = \alpha w_1(n) + \mu x_1'(n) e(n) \tag{19}$$

where $x_0'(n)$ and $x_1'(n)$ are the filtered reference signals using the estimated dynamics of secondary path S(z) as the filter. μ is the constant convergence rate and α is the leakage factor with a range between 0 to 1. As shown in figure 1 and 3, in an integrated FBN control system, S(z) is the dynamics between the input of the active actuator $y(n)$ and the measured pressure $e(n)$. $e(n)$ is the residual pressure signal:

$$e(n) = d(n) - y(n) \tag{20}$$

The FXLMS algorithm has been successfully implemented on a digital switched inertance hydraulic system to attenuate pressure pulsations [11, 15]. However, it is found that the conventional FXLMS could converge slowly if the constant convergence rate was not well chosen. To achieve faster convergence speed of the controller, a variable step-size filtered-X LMS (VSS-FXLMS) algorithm is used for the proposed integrated control system. The algorithm has been investigated by Huang *et al* theoretically [30]. They concluded that the VSS-FXLMS converges much faster but requires more computations compared with the conventional FXLMS algorithm.

For the variable step-size FXLMS algorithm, the adaptive weights are iterated using a variable step size $\mu(n)$ given by:

$$w_0(n+1) = \alpha w_0(n) + \mu(n) x_0'(n) e(n) \tag{21}$$

$$w_1(n+1) = \alpha w_1(n) + \mu(n) x_1'(n) e(n) \tag{22}$$

and $\mu(n)$ is [23]:

$$\mu(n) = \xi\mu(n-1) + \eta e(n) x_0'(n) e(n-1) x_0'(n-1) \tag{23}$$

Where ξ is a positive constant very close to 1 and η is a very small user-defined step size to confine $\mu(n)$ within the stability bounds.

The single frequency FXLMS algorithm can be configured to cancel multiple frequencies by setting additional filters in parallel. Figure 4 shows the schematic of multiple-frequency FBN cancellation system using adaptive notch filters with a variable step-size FXLMS algorithm. The piezo actuator is used to generate the anti-phase control flow rate and seen as the secondary path S(z) including the couplings connecting to the main fluid path. M is the number of the frequencies. The reference inputs are given by:

$$x_{m,0}(n) = \sin(2\pi m f_0 n\Delta t) \tag{24}$$

$$x_{m,1}(n) = \cos(2\pi m f_0 n\Delta t) \qquad m = 1, 2, \ldots M \tag{25}$$

The cancelling signal is a sum of m adaptive filter outputs

$$y(n) = \sum_{m=1}^{M} y_m(n), \; m = 1, 2, \ldots, M \tag{26}$$

$$y_m(n) = w_{m,0}(n) x_{m,0}(n) + w_{m,1}(n) x_{m,1}(n), \; m = 1, 2, ..., M \tag{27}$$

The adaptive weights are iterated using variable step sizes given by:

$$\mathbf{w}_0(n+1) = \alpha \mathbf{w}_0(n) + \boldsymbol{\mu}(n) x_0'(n) e(n) \tag{28}$$

$$\mathbf{w}_1(n+1) = \alpha \mathbf{w}_1(n) + \boldsymbol{\mu}(n) x_1'(n) e(n) \tag{29}$$

$$\boldsymbol{\mu}(n) = \xi\boldsymbol{\mu}(n-1) + \eta e(n) \mathbf{x}_0'(n) e(n-1) \mathbf{x}_0'(n-1) \tag{30}$$

where $\mathbf{w}_0(n) = [w_{1,0}(n)\ w_{2,0}(n) \ldots w_{m,0}(n)]$, $\mathbf{x}_0'(n) = [\ x_{1,0}'(n)\ x_{2,0}'(n) \ldots x_{m,0}'(n)\ ]$.

The Fast Block Least Mean Square (FBLMS) algorithm is used as the on-line identification filter to identify the characteristics of the secondary path $S(z)$. FBLMS is operating in the frequency domain. Compared with the time-domain on-line identification methods, the FBLMS can substantially improve the robustness of the identification process. The detailed derivation and analysis of the FBLMS algorithm can be found in Ref. [16].

We designed the active noise attenuator using a commercial preloaded piezo actuator P-225.40 (customized), together with a high-power amplifier E-481 from Physik Instrumente with a free displacement range of $0 \le x_p \le 60$ μm. The preload force is 2 kN. The linearized equation for the actuator force, excluding dynamic effects, is given by [31]:

$$F_a = k_v V - k_x x_p \tag{31}$$

where V is the applied voltage, x_p is the extension of the actuator, k_x is the actuator stiffness, and k_v is a force/voltage coefficient. Equation 31 shows the force generated by the actuator is dependent on its displacement, with a maximum compressive blocking force of 12.5 kN.

The designed active piezoelectric actuator (with housing) is shown in Figure 5. The actuator provides FBN attenuation by controlling the dynamic volume in the flow path. A pressure transducer is arranged downstream to measure the error signal $e(n)$. An integrated position sensor is used to measure and monitor the displacement of the piezoelectric actuator. An initial applied voltage on the piezoelectric actuator was 400 V, which determines the initial flow volume of the actuator, as shown in Figure 5 (a). Figure 6 shows the relationship between the voltage and the displacement. When the controller is switched on and

driven by the cancelling signal $y(n)$, the actuator extends and retracts, resulting in the expansion and reduction of flow volume, which is used to attenuate the FBN $d(n)$. The voltage-dependent displacement curves of piezo actuators show nonlinearity in the form of hysteresis, but this can be compensated by using feedback position control.

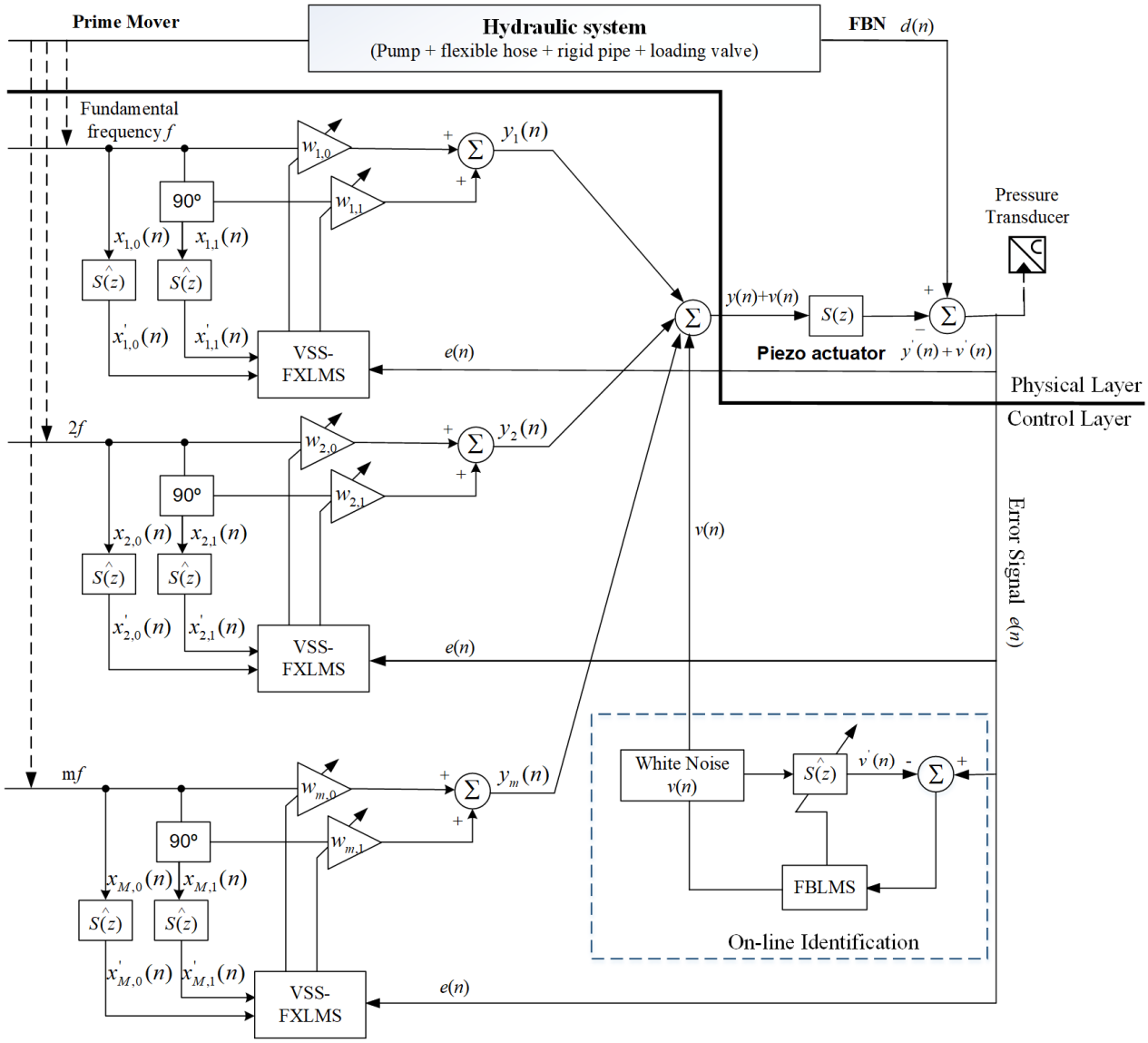

FIGURE 4. Block diagram of ANC for FBN cancellation using VSS-FXLMS algorithm

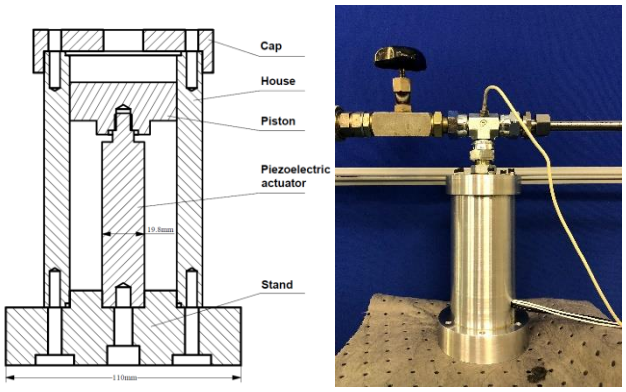

(a) (b)

FIGURE 5. (a) Schematic of the designed piezoelectric actuator (b) Photograph of the actuator

The electrical capacitance of the actuator is 1300 *nF* (±20%), which limits the speed of build-up of the applied voltage. The dynamic response of the piezo actuator P-225.40 amplifier and actuator is modelled as a second-order system based on the manufacturer's data sheets [32]. The bandwidth is modelled as 1000 Hz (6283 rad/s) and the damping ratio is 0.8.

$$S(s) = \frac{\omega^2}{s^2 + 2\zeta\omega s + \omega^2} \tag{32}$$

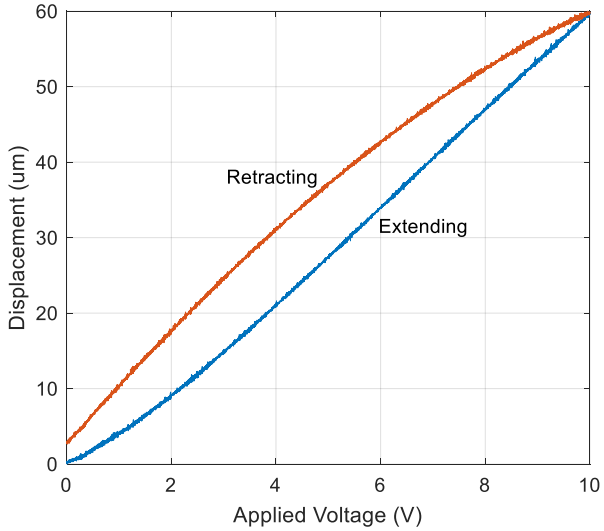

FIGURE 6. Piezo displacement and amplifier input voltage V_a (piezo actuator voltage $V = 100V_a$)

3. SIMULATION RESULTS

The Fast Block Least Mean Square (FBLMS) algorithm is used for the on-line identification filter to identify the characteristics of the secondary path $S(z)$. The identification result of the secondary path $S(z)$ is shown in Figure 7, where the length of the FBLMS filter is 512. The theoretical impulse response of the secondary path achieved by using an impulse flow rate with an amplitude of 1×10^{-4} m^3/s was used for comparison of the identification results. The FBLMS identification result agreed well with the theoretical impulse response. The simulated mean pressure is 100 bar and the delivery flow is 14 L/min. A resistance of 3.75×10^{10} $Pa/(m^3/s)$ is applied to represent the loading system. Parameters for simulation are listed in Table 2.

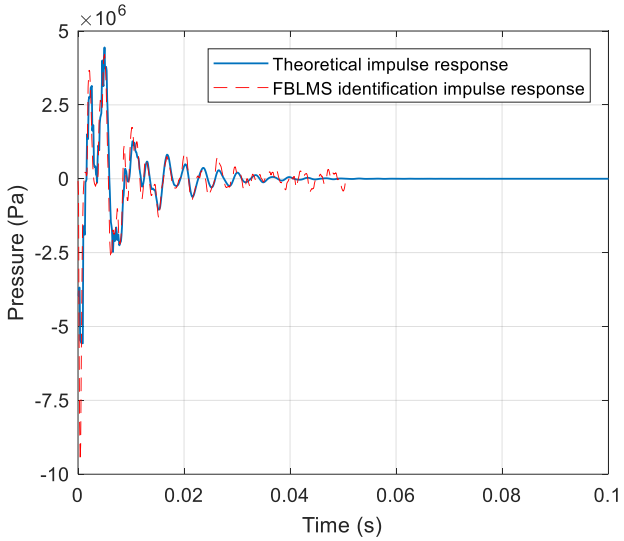

FIGURE 7. Secondary path $S(z)$ identification

An external gear pump which has ten teeth on each gear operating at a speed of 960 rpm is modelled in simulation. The fundamental frequency of the pressure ripple in this case is 160 Hz (960/60 rps ×10 teeth = 160Hz). The FBN cancellation results for the frequency of 160 Hz in the time domain and frequency domain are shown in Figure 8. The active attenuator was switched on at 2s and the simulated mean pressure was 100 bar. Figure 8 (a) shows the FBN cancellation in the time domain where the pressure ripples have been successfully attenuated within 1 s. To ensure the accuracy of the identification results, an extra 2 s was used for identification before switching on the active controller. Both conventional fixed coefficient FXLMS and the VSS-FXLMS were used for the active attenuator, which is very effective to FBN cancellation. The active controller with the VSS-FXLMS algorithm converged 2.7 times faster than the controller using the conventional FXLMS with a constant step size. Five dominant harmonics are considered in the attenuation in the frequency domain. The magnitude of the ripple at the frequency of 160 Hz is 20 bar. This simulates a gear pump with ten teeth on each gear driven at a speed of 960 rpm and with a delivery flow rate of 14L/min. The Hanning window was used for signal processing in the frequency domain. The lengths of the tuned hose are 1.1 m and 1.7 m.

The average ripple cancellation at five harmonics with tuned hoses was about 70 dB, as shown in figure 8 (b) and (c), where the pressure pulsations at these frequencies are effectively attenuated using the active controller, and the high-frequency ripples are reduced by the tuned passive hoses (numbers in dB

shown in Figure 8 are the total cancellations). Table 3 listed the ripple amplitudes before and after the cancellation.

TABLE 2. Simulation parameters

Hose length (m)	1.1 and 1.7
Fluid density (kg/m^3)	870
Internal diameter of the hose (mm)	12.5
Kinematic viscosity (cSt)	16
Bulk modulus (Pa)	1.336×10^9
Diameter of the rigid pipe (mm)	10
Pipe length (m)	1

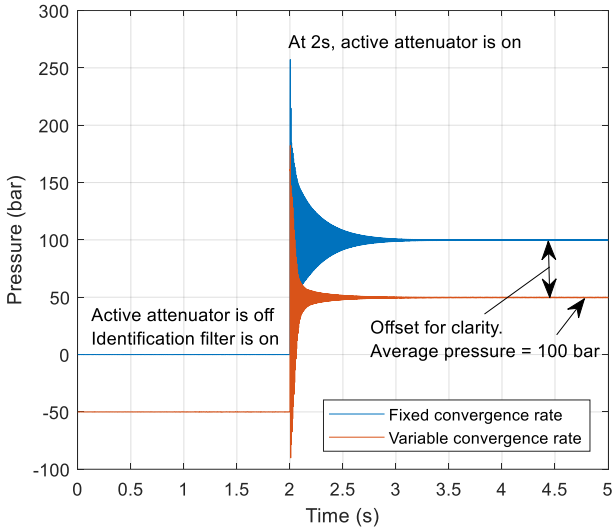

(a) Time domain (1.1m hose)

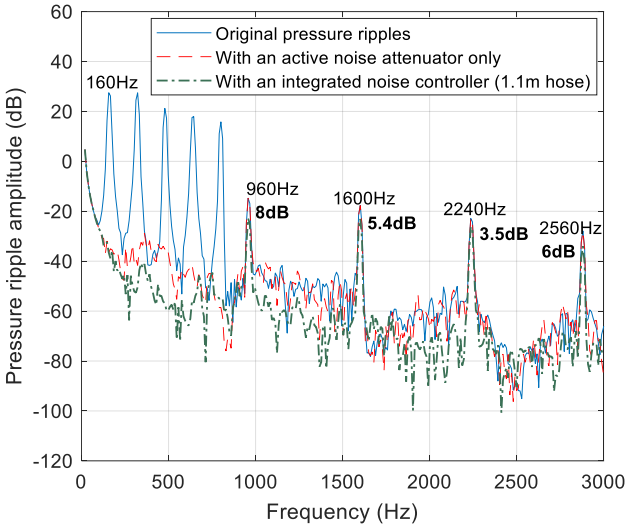

(b) Frequency domain (1.1m hose)

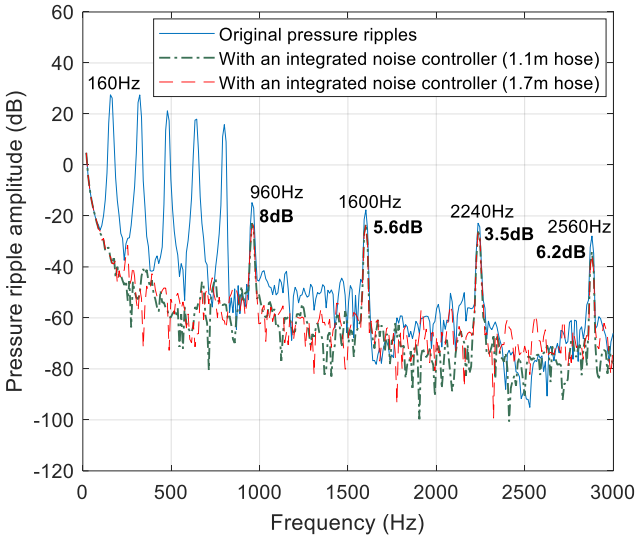

(c) Frequency domain (1.7m hose)

FIGURE 8. Simulated pressure pulsation cancellation using the integrated control method

TABLE 3. Simulated pressure ripple amplitude before and after cancellation

Frequency (Hz)	160	320	480	640	800
Before cancellation (bar)	20	10	10	10	5
Before cancellation (dB)	27.5	27.5	21.2	18.0	15.8
After cancellation (1.1m hose) (dB)	-36.5	-50.4	-56.8	-56.7	-54.6
After cancellation (1.7m hose) (dB)	-36.0	-48.1	-54.1	-66.3	-61.2
Total reduction (dB)	64	76-78	75-78	75-84	70-77

Figure 9 shows the adaptive weights w_1 and w_2 at the frequency of 160 Hz using the variable and constant step-size FXLMSs. The active controller was switched on at 2s. The constant convergence rate μ, 5×10^{-21} is used for the fundamental frequency cancellation. The variable step size $u(t)$ is shown in Figure 10, where $u(t)$ increased to its peak at around 3s to achieve high convergence speeds, then decreased to a small value (ideally converging to a constant value when $e(t)$ is very close to zero). Figure 9 also proved that the variable step-size FXLMS algorithm converged 2.7 times faster than using the constant step-size FXLMS algorithm.

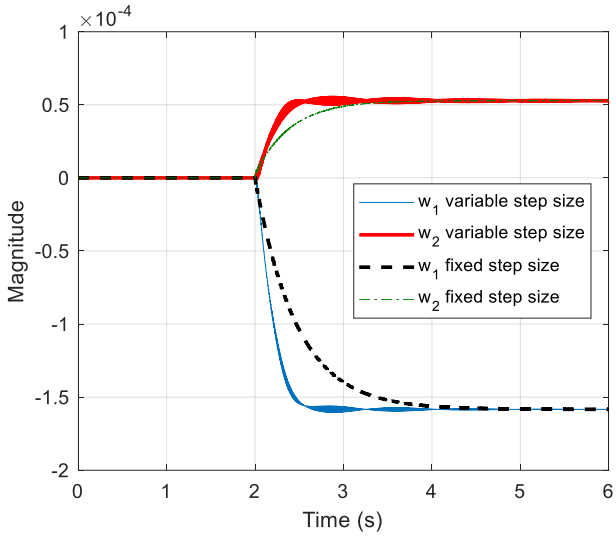

FIGURE 9. Adaptive weights for the cancellation at the fundamental frequency of 160 Hz

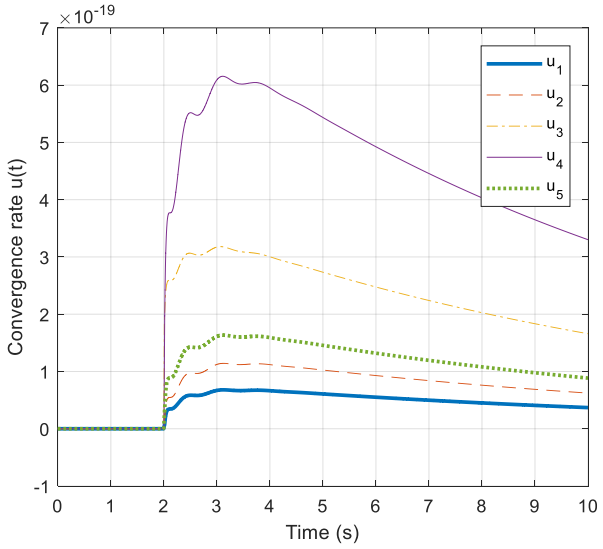

FIGURE 10. Variable step size $u(t)$

4. EXPERIMENTAL VALIDATION

Figure 11 shows the experimental test rig which consists of an external gear pump with a displacement of 10.8 cm^3/rev acting as the primary noise source, a flexible hose of 1.1m, a rigid pipe of 1m and a simple restrictor acting as the load. The gear pump has ten teeth on each gear and the speed is 960 rpm giving a flow rate of 9 L/min. The loading pressure is 40 bar. The active attenuator is implemented on the Speedgoat Real-time Simulation and Testing Platform, which is used to cancel the dominant harmonics at the frequencies of 160 Hz, 320 Hz, 480 Hz, 640 Hz and 800 Hz. The flexible hose is used to attenuate the higher-frequency pressure pulsations.

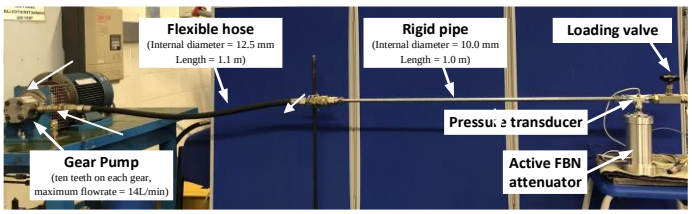

FIGURE 11. Experimental test rig

The length of the online FBLMS identification filter was 256 and the sample time step was 0.1ms. The amplitude and phase of the estimated secondary path $\hat{S}(z)$ are shown in Figure 12, where the amplitude agrees very well with the theoretical curve achieved using the Fast Fourier Transform. There is a phase deviation at the higher frequencies (>1300 Hz), which can be compensated by using a filter with a longer length filter. It is believed that the length of 256 cannot fully describe the characteristics of the secondary path $S(z)$. However, the longer length filter requires more computation. Therefore, there is a trade-off between the accuracy and the computation required for the secondary path identification.

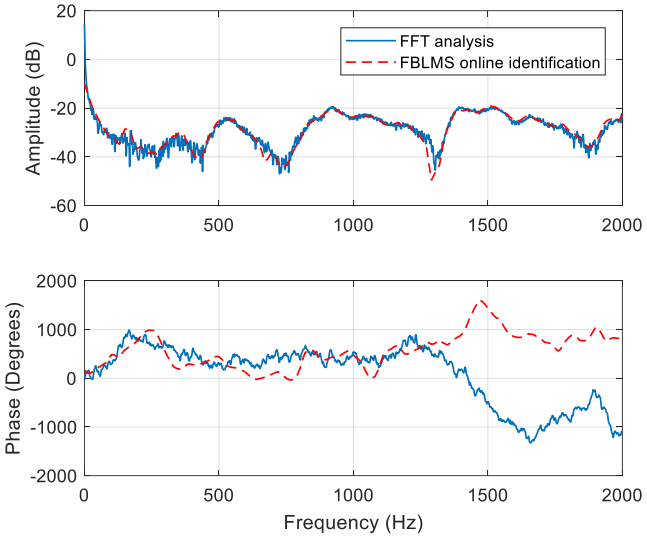

FIGURE 12. Estimated secondary path $\hat{S}(z)$ identification result

In this work, the dominant frequencies considered are less than 1000 Hz, thus the estimated $\hat{S}(z)$ is sufficient for the application.

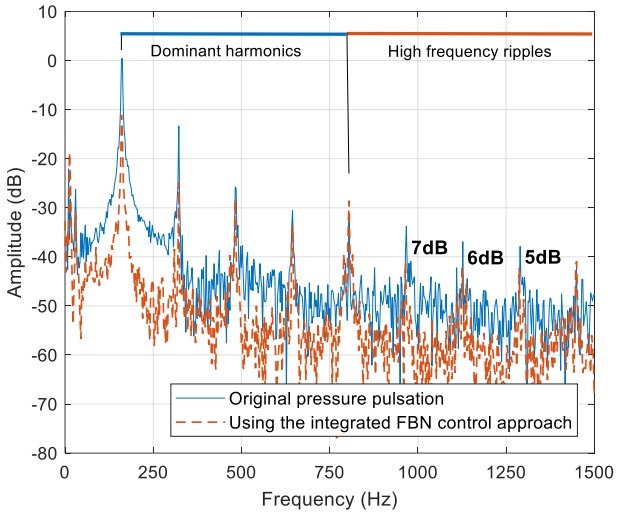

FIGURE 13. Experimental pressure pulsation cancellation at five harmonics using the proposed integrated approach

Figure 13 shows the pressure ripple attenuation in the frequency domain. The reductions were 11 dB and 12 dB at the frequencies of 160 Hz and 320 Hz, respectively. The average cancellation at the five dominant harmonics (160 Hz, 320 Hz, 480 Hz, 640 Hz and 800 Hz) was over 7 dB, as listed in Table 4. However, the pressure amplitude increased by 3 dB at the frequency of 800 Hz, which might be caused by system nonlinearity or a resonance effect. In addition, the bandwidth of the piezoelectric actuator could limit the performance of the active attenuator.

For the high-frequency range, the tuned flexible hose effectively cancelled pressure ripples with an average attenuation of 6 dB. The experimental results proved the principle and feasibility of the proposed integrated FBN cancellation system. Continuous work is focused on the investigation of controller performance, stability, hose tuning strategies, effect of varying operating conditions and related applications of the designed systems.

TABLE 4. Pressure ripple amplitude before and after cancellation in experiments

Frequency (Hz)	160	320	480	640	800
Before cancellation (dB)	0.3	-13	-26	-31	-32
After cancellation (dB)	-11	-25	-28	-34	-29
Total reduction (dB)	11	12	2	3	-3

5. DISCUSSION

The novel integrated active and passive control method can effectively attenuate FBN over a wide range of frequencies by integrating the active FBN attenuator and passive flexible hoses. In this work, the hose parameters were well tuned and investigated in the frequency domain to ensure very good damping performance. The knowledge of hose properties is essential for the frequency-domain analysis and the static and dynamic properties of the hoses are needed. The inaccuracy of the hose properties could cause uncertainty of the tuning parameters. Alternatively, a time-domain hose model could be a solution for the tuning process by using easily measured hose parameters including hose length, inner and outer diameters, mass per unit length, reinforcement diameter and estimated bulk modulus. The time-domain hose model could be used to predict hose dynamics directly without the precise static and dynamic properties of the hoses achieved from the frequency-domain analysis.

A ten-teeth gear pump was used as the primary noise source in experiments. Unlike well-designed gear pumps, larger pressure pulsations are generated by axial piston pumps because the sudden fluid compression process within axial piston pumps. The flow ripple from piston pumps is also highly dependent on the mean delivery pressure, which could significantly affect the performance of the active attenuator. Applying the integrated method to axial piston pump pressure pulsation cancellation will be the subject of future research.

In addition, higher operating pressures will be applied for the gear pump tests, in which larger pressure pulsation amplitudes are expected. In this case, higher force generated from the piezo actuator is needed and larger structure-borne noise disturbance is expected, which provides a good opportunity for investigating the controller's stability. We will investigate the variable time-step FXLMS for FBN attenuation in terms of the performance and stability of the algorithm.

We had successfully used a piezoelectric valve for FBN attenuation in a digital hydraulic system at Bath in 2012 [11]. Using a valve as an active controller by bleeding-off the primary flow rate creates a power loss. In this work, we used the flow volume created by a piezoelectric actuator rather than bleeding the flow rate. Good FBN cancellations were achieved. Compared to the valve bleeding-off technique, the use of actuator is less effective in terms of noise cancellation level. The main reason is that a valve introduces a small orifice, which can effectively damp the higher frequency dynamics of the system and enhance the stability of the controller. Secondly, the system pressure is limited by the preload force of the piezoelectric actuator, whilst it can be completely independent of the preload force with a well-designed valve. The major advantage of using an actuator is that much less energy loss is consumed compared to valve-controlled approach. We believe that there is an optimal actuator piston area and an optimal location of the error pressure transducer for the most efficient attenuation, and this will be investigated in the future.

6. CONCLUSIONS

The novel integrated control method can effectively reduce FBN over a wide range of frequencies. It is the first time that active and passive FBN control methods have been integrated to form a high-bandwidth hybrid noise controller. The simulated and experimental results show effective FBN attenuation and prove the principle and feasibility of the approach. The variable step-size FXLMS algorithm provides very fast convergence of the active attenuator. Using a piezoelectric actuator to modulate

volume rather than bleed-off flow, power is not wasted unlike the active valve-controlled approach. It is concluded that the active attenuator with passive flexible hoses can construct an effective, energy-efficient and practical solution for FBN attenuation. The reduction in FBN can contribute towards reductions in overall air-borne noise and structure-borne noise levels, which provides an effective approach to reduce noise pollution from hydraulic machines. This improves the quality of life of both users and bystanders.

ACKNOWLEDGEMENTS

This work was supported by the UK Engineering and Physical Sciences Research Council under grant number EP/P022022/1, together with the RAEng/The Leverhulme Trust Senior Research Fellowship, UK, grant number LTSRF1819\15\16, the RAEng Proof-of-Concept Award PoC1920/15. The authors would like to thank Dr D Nigel Johnston who provided the time-domain hose model and the software tool *Prasp* for this research.

REFERENCES

[1]. Pan, M., Ding, B., Yuan, C., Zou, J. and Yang, H., 2018, November. Novel Integrated Control of Fluid-Borne Noise in Hydraulic Systems. In *BATH/ASME 2018 Symposium on Fluid Power and Motion Control*. American Society of Mechanical Engineers Digital Collection.

[2]. Zhang, J., Xia, S., Ye, S., Xu, B., Zhu, S., Xiang, J. and Tang, H., 2019. Sound quality evaluation and prediction for the emitted noise of axial piston pumps. Applied Acoustics, 145, pp.27-40.

[3]. Chao, Q., Zhang, J., Xu, B., Huang, H. and Pan, M., 2019. A review of high-speed electro-hydrostatic actuator pumps in aerospace applications: challenges and solutions. Journal of Mechanical Design, 141(5), p.050801.

[4]. Pan, M, Johnston, DN, Plummer, AR, Kudzma, S & Hillis, AJ 2014, Theoretical and experimental studies of a switched inertance hydraulic system including switching transition dynamics, non-linearity and leakage. Proceedings of the Institution of Mechanical Engineers, Part I: Journal of Systems and Control Engineering, vol. 228, no. 10, pp. 802-815.

[5]. Pan, M, Johnston, D, Plummer, A, Kudzma, S & Hillis, A 2014, 'Theoretical and experimental studies of a switched inertance hydraulic system' Proceedings of the Institution of Mechanical Engineers, Part I: Journal of Systems and Control Engineering, vol. 228, no. 1, pp. 12-25.

[6]. Pan, M., Johnston, D.N. and Plummer, A., 2016. Hybrid fluid-borne noise control in fluid-filled pipelines. In *Journal of Physics: Conference Series* (Vol. 744, No. 1, p. 012016). IOP Publishing.

[7]. Yuan, C, Pan, M & Plummer, A 2020, 'A Review of Switched Inertance Hydraulic Converter Technology', *Journal of Dynamic Systems, Measurement and Control: Transactions of the ASME*. https://doi.org/10.1115/1.4046103.

[8]. Pan, M & Plummer, A 2018, 'Digital switched hydraulics', Frontiers of Mechanical Engineering, vol. 13, no. 2, pp. 225-231.

[9]. Pan, M & Yang, H 2015, 'Engineering research in fluid power: a review', Journal of Zhejiang University SCIENCE A, vol. 16, no. 6, pp. 427-442.

[10]. Inline Pulse-Tone™ Shock Suppressors, Parker Hannifin, https://ph.parker.com/gb/en/accumulators.

[11]. Pan, M 2017, 'Adaptive Control of a Piezoelectric Valve for Fluid-borne Noise Reduction in a Hydraulic Buck Converter', *Journal of Dynamic Systems, Measurement and Control: Transactions of the ASME*, vol. 139, no. 8, 081007.

[12]. Rebel, J. 1977. Active liquid noise-suppressions in oil hydraulics (in German). VDI-Z., 119, 937–943.

[13]. Maillard, J, Lago, T. and Fuller, C. 1999. Fluid wave actuator for the active control of hydraulic pulsations in piping systems. *Proceedings of the International Modal Analysis Conference IMAC*, pp. 1806-1812.

[14]. Wang L and Johnston DN. 2008 Adaptive attenuation of narrow band fluid borne noise in a simple hydraulic system. *In: Bath/ASME Symposium on Fluid Power and Motion Control*. Bath. University of Bath, pp. 357-368.

[15]. Pan, M 2012, Active Control of Pressure Pulsation in a Switched Inertance Hydraulic System, Ph.D Thesis, University of Bath.

[16]. Kuo, S.M. and Morgan, D., 1995. Active noise control systems: algorithms and DSP implementations. John Wiley & Sons, Inc.

[17]. Xu, B., Ye, S., Zhang, J. and Zhang, C., 2016. Flow ripple reduction of an axial piston pump by a combination of cross-angle and pressure relief grooves: Analysis and optimization. Journal of Mechanical Science and Technology, 30(6), pp.2531-2545.

[18]. Ye, S.G., Zhang, J.H. and Xu, B., 2018. Noise reduction of an axial piston pump by valve plate optimization. Chinese Journal of Mechanical Engineering, 31(1), p.57.

[19]. Lyu, F., Ye, S., Zhang, J., Xu, B., Huang, W., Xu, H. and Huang, X., 2020. Theoretical and Simulation Investigations on Flow Ripple Reduction of Axial Piston Pumps Using Nonuniform Distribution of Pistons. Journal of Dynamic Systems, Measurement, and Control, 143(4).

[20]. Longmore, D.K., 1977, The transmission and attenuation of fluid borne noise in hydraulic hose. In IMechE *Conference on Quite Oil Hydraulic Systems*, London, pp. 127-138.

[21]. Johnston, D.N., 2006. A time-domain model of axial wave propagation in liquid-filled flexible hoses. *Proceedings of the institution of mechanical engineers, Part I: Journal of systems and control engineering*, *220*(7), pp.517-530.

[22]. Drew, J.E., Longmore, D.K. and Johnston, D.N., 1997. Measurement of the longitudinal transmission characteristics of fluid-filled hoses. *Proceedings of the Institution of Mechanical Engineers, Part I: Journal of Systems and Control Engineering*, *211*(3), pp.219-228.

[23]. Drew, J.E., Longmore, D.K. and Johnston, D.N., 1998. Theoretical analysis of pressure and flow ripple in flexible hoses containing tuners. *Proceedings of the Institution of Mechanical Engineers, Part I: Journal of Systems and Control Engineering*, *212*(6), pp.405-422.

[24]. Taylor, S.E.M., 1998. Development of numerical models for hydraulic pipelines and flexible hoses (PhD Thesis, University of Bath).

[25]. Way, T.M., 2004. The use of hoses and hose inserts to reduce pressure ripple in hydraulic circuits, Ph.D Thesis, University of Bath.

[26]. Johnston, D.N., Way, T.M. and Cone, K.M., 2010 Measured dynamic properties of flexible hoses. *Journal of Vibration and Acoustics*, 132(2), p.021011.

[27]. Johnston, D.N., 2007 Pressure ripple analysis software Package PRASP: user guide and reference manual. *Centre for Power Transmission and Motion Control*, University of Bath. UK.

[28]. Widrow, B. and Hoff, M.E., 1960. Adaptive switching circuits (No. TR-1553-1). Electronics Labs, Stanford University CA, WES-CON Conv. Rec., 4(1), pp. 96–104.

[29]. Haykin, S., 1996, Adaptive Filter Theory, Prentice Hall, Eaglewood Cliffs, NJ.

[30]. Huang, B., Xiao, Y., Sun, J. and Wei, G., 2013. A variable step-size FXLMS algorithm for narrowband active noise control. *IEEE transactions on audio, speech, and language processing*, *21*(2), pp.301-312.

[31]. Branson, D. T., Johnston, D. N., Tilley, D. G., Bowen, C. R., and Keogh, P. S., 2010, Piezoelectric Actuation in a High Bandwidth Valve, Ferroelectrics, 408(1), pp. 32–40.

[32]. P-225 PICA Power Piezo Actuators datasheet and E-482 PICA High-Performance Piezo Amplifier datasheet, PI Physik Instrument LT.

Table captions

Figure captions